Recovery of actinides from actinide-aluminium alloys by chlorination: Part II

Pavel Soucek, Laurent Cassayre, Rachel Eloirdi, Rikard Malmbeck, Roland Meier, Christophe Nourry, Benoit Claux, Jean-Paul Glatz

HAL Id: hal-00948022

https://hal.science/hal-00948022

Submitted on 17 Feb 2014

Recovery of actinides from actinide–aluminium alloys by chlorination: Part II

P. Souček [a,*], L. Cassayre [b], R. Eloirdi [a], R. Malmbeck [a], R. Meier [a], C. Nourry [a], B. Claux [a], J.-P. Glatz [a]

[a] European Commission, JRC, Institute for Transuranium Elements, Postfach 2340, 76125 Karlsruhe, Germany
[b] Laboratoire de Génie Chimique (LGC), Département Procédés Electrochimiques, CNRS-UMR 5503, Université de Toulouse III – Paul Sabatier, 31062 Toulouse Cedex 9, France

A chlorination route is being investigated for recovery of actinides from actinide–aluminium alloys, which originate from pyrochemical recovery of actinides from spent metallic nuclear fuel by electrochemical methods in molten LiCl–KCl. In the present work, the most important steps of this route were experimentally tested using U–Pu–Al alloy prepared by electrodeposition of U and Pu on solid aluminium plate electrodes. The investigated processes were vacuum distillation for removal of the salt adhered on the electrode, chlorination of the alloy by chlorine gas and sublimation of the $AlCl_3$ formed. The processes parameters were set on the base of a previous thermochemical study and an experimental work using pure UAl_3 alloy. The present experimental results indicated high efficiency of salt distillation and chlorination steps, while the sublimation step should be further optimised.

1. Introduction

A chlorination route is under investigation at ITU for recovery of actinides (An) from actinide–aluminium (An–Al) alloys, which originate from pyrochemical treatment of spent metallic nuclear fuel by electrochemical methods in molten LiCl–KCl [1,2]. The background, principles and thermodynamic calculation related to the method have been described in detail in the previous work [3]. The present work was focused on a laboratory-scale demonstration of the process using U–Pu–Al alloy prepared by electrodeposition of U and Pu on solid aluminium plate electrodes by electrorefining of U–Pu–Zr alloy in the molten salt. All the most important steps of the chlorination route were tested, i.e., vacuum distillation for removal of the salt adhered on the electrode, chlorination of the alloy by chlorine gas and sublimation of the $AlCl_3$ formed. The tested experimental conditions were derived from the previous thermochemical study on the process and from the chlorination experiments with UAl_3 alloy [3]. The conditions were set to provide complete chlorination, but preventing volatilisation of the present actinides. All the process steps were evaluated on the basis of X-ray diffraction (XRD) analyses of the reacting material, combined in some cases with inductively-coupled plasma mass spectrometry (ICP-MS) or optical emission spectrometry (ICP-OES) and scanning electron microscopy coupled with energy-dispersive X-ray spectroscopy (SEM-EDX) measurements.

* Corresponding author. Tel.: +49 7247951124.
  E-mail address: pavel.soucek@ec.europa.eu (P. Souček).

2. Preparation of U–Pu–Al alloys

The initial material was prepared by potentiostatic electrorefining of U–Pu–Zr alloy (71–19–10 wt.%, respectively, ITU stock material) in LiCl–KCl eutectic melt (Aldrich 99.99%) using Al plate cathodes (99.999%, Alfa Aesar). Three runs were carried out at a temperature of 450 °C, yielding alloys with different actinide content due to development of actinides concentrations in the melt. A detailed description of the electrorefining process can be found elsewhere [4].

2.1. Experimental – electrorefining

The electrorefining runs were carried out in a glovebox under purified Ar atmosphere (<5 ppm of moisture and oxygen). The electrolyte consisted of LiCl–KCl eutectic melt containing UCl_3 and $PuCl_3$ (1.78 and 0.62 wt.% metal, respectively) was prepared by chemical oxidation of the U–Pu–Zr alloy by $BiCl_3$ according to the procedure described in [5]. The formed Bi metal was collected in a Bi pool at the bottom of an alumina crucible. After the reaction was completed, which was evidenced by electrochemical measurement, the melt was slowly cooled to solid state, the crucible was broken and the Bi pool was mechanically removed. The recovered melt was transferred to a new alumina crucible and used as the electrolyte. The U–Pu–Zr alloy was loaded in a Ta basket and connected as an anode. Cathodes were made of Al plates with dimensions of the immersed parts $10 \times 10 \times 0.5$ mm. The reference electrode used was an Ag/LiCl–KCl–AgCl (1 wt.%) prepared in a Pyrex glass tube. PAR 273 potentiostat with EG&G

M270 electrochemical software was used to control the electrorefining.

2.2. Electrorefining runs

A potential of -1.30 V vs. Ag/AgCl, which is suitable for deposition of both actinides on solid aluminium [6,7], was used for all electrorefining runs. The value of passed charge was selected in a way to produce deposits using approximately 70–80% of Al plates capacity, assuming current efficiency 80% and formation of $AnAl_3$ alloys. Typically, the current density decreased during the runs from -15 to -6 mA/cm^2 due to the slowing down of intermetallic diffusion of An and Al through the An–Al alloy formed on the electrode surface. The development of current in dependency on the passed charge is shown in Fig. 1 for a partly exceptional case in run 2. The initial current decrease was followed by a stable current and in the final phase even increasing current. It can be explained by co-deposition of Zr dissolved from the anode at the later stage of this run, as the deposition potential of Zr is approximately 250 mV more positive than for U, which could yield higher deposition rate and consequently the increasing current. Another explanation can be based on the increase of the surface area in this run due to a different morphology of Zr containing deposit, but this feature was not observed in this particular case, when only 0.6 wt.% of Zr was co-deposited.

The concentration profile, shown in Fig. 2 (left), indicates an increasing concentration of Pu in the electrolyte. U and Pu are congruently electrochemically dissolved from the U–Pu–Zr alloy [8], but U is electrodeposited predominantly on Al due to its more anodic deposition potential in comparison with Pu [6,7]. It led to higher consumption of U from the electrolyte, i.e., decreasing of U concentration and increase of Pu concentration. The U concentration increase observed after run 1 is probably not correct due to possible cross contamination of the ICP-MS sample during preparation in U contaminated glove boxes.

Due to substantially more positive electrode potential of Zr electrochemical oxidation than these of U and Pu, Zr is generally not dissolved in the melt until major part of the actinides are removed from the U–Pu–Zr alloy [8]. During runs 1 and 2 (Fig. 2_right) about 70 wt.% of U and Pu was removed from the initial alloy and it finally led to partial co-dissolution of Zr to the melt. Before run 3, a new pin of the U–Pu–Zr alloy was thus added to the anode basket to reduce the Zr content in the melt and to provide conditions for more efficient preparation of the last required An–Al alloy deposit. The ICP-MS results confirmed full reduction of the dissolved Zr, however they also showed an unexpected decrease of U and Pu concentration in the melt (Fig. 2_left). It
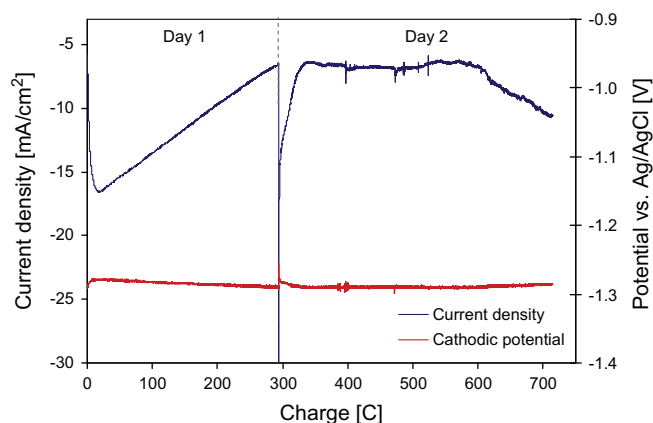
indicates relatively high uncertainty of the ICP-MS in this case, nevertheless the general trends in the concentration developments are well illustrated by these results. The expected development of anodic material composition during the runs is shown in Fig. 2 (right).

2.3. Material characterisation

After the required charge was passed, each electrode was left above the melt surface for several hours at working temperature to let some adhered salt drop off the surface. In all cases, shiny metallic-looking deposit was obtained, homogeneously distributed and well adhered on the electrode surface. A cross section of the electrode with the deposit from run 2 is shown in Fig. 3a.

The deposit was mechanically scraped without washing, homogenised by fine grinding in a mortar and sampled for XRD and ICP-MS analyses.

The mass balance of the electrodeposition runs based on ICP-MS results is summarised in Table 1. The masses of An in the deposits were corrected from the evaluated An content in the adhered salt. To illustrate the achieved capacity of Al to take up actinides, a loading of each electrode was calculated using a mass ratio of the deposited An and the immersed part of Al electrode. The maximum possible An/Al ratio was derived from the alloy composition An–Al$_3$, typically formed during the electrorefining process [5].

Consistently with the concentration profiles presented in Fig. 2, the increasing content of Pu in the product along the three runs was caused by its increasing concentration in the salt. Since the equilibrium potential (E_{eq}) is concentration dependent according to Nernst law, at the later stage of the process, the overvoltage between E_{eq} and the deposition potential E_{dep}, is increasing. Therefore, according to Butler–Volmer equation, higher portion of Pu was co-deposited with U.

Somewhat lower current efficiency achieved in run 2 might be explained by co-deposition of Zr on the Al cathode. A deterioration of An–Al deposits macroscopic structure and lowering of current efficiency has been positively observed in previous electrorefining experiments for the cases of Zr co-dissolution and co-deposition [5]. A higher salt content detected in the corresponding deposit by ICP-MS and also the highest mass loss of the material during distillation supports this explanation (see Section 3.3.1 below); however no worsening of the deposit macroscopic quality was observed.

The X-ray diffraction analyses have been performed on a Bruker D8 Bragg-Brentano Advance diffractometer (Cu Kα1 radiation) equipped with a Lynxeye Linear Position Sensitive detector. The operation conditions were 40 kV and 40 mA. Powder diffraction patterns were recorded at room temperature across an angular range $10° \leqslant 2\theta \leqslant 120°$. The phase quantification procedure involved in the identification of the different phases was done using the software Match (Crystal Impact) and quantification of phases of all data sets was done by the full profile Rietveld method implemented in the software Topas version 4.1. (Coelho, 2007). The starting structure models were adopted from the Inorganic Crystal Structure Data Base (ICSD). The computations involved adjustment of the scale factors, pattern background polynomial parameters, the sample displacement, lattice parameters and peak profile options. The refinement of preferred orientation was done by the March–Dollase Model with an order of 4–8. Depending on the analyses conditions, scan time and sample preparation, the detection limit of X-ray diffraction can be of the order of 1–5 wt.%. Due to close crystallographic parameters of UAl$_x$ and PuAl$_x$ or a solid solution of both phases, XRD cannot distinguish them, as the differences in the positions of the corresponding diffraction peaks are below resolution of the instrument. The same is valid for chlorides UCl$_3$ and PuCl$_3$. To determine the U/Pu ratio and to extend the

Fig. 1. Development of current density (upper line) with the passed charge during electrochemical preparation of U–Pu–Al alloy, run 2.
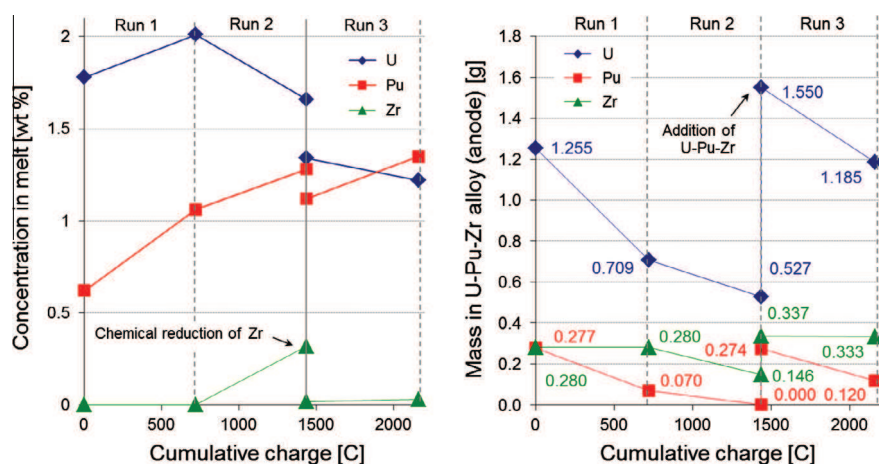
Fig. 2. Concentration profile of U, Pu and Zr in the melt (left) and masses of these elements in the anodic material calculated on the base of ICP-MS analyses of the melt and deposits during the electrorefining runs (right).
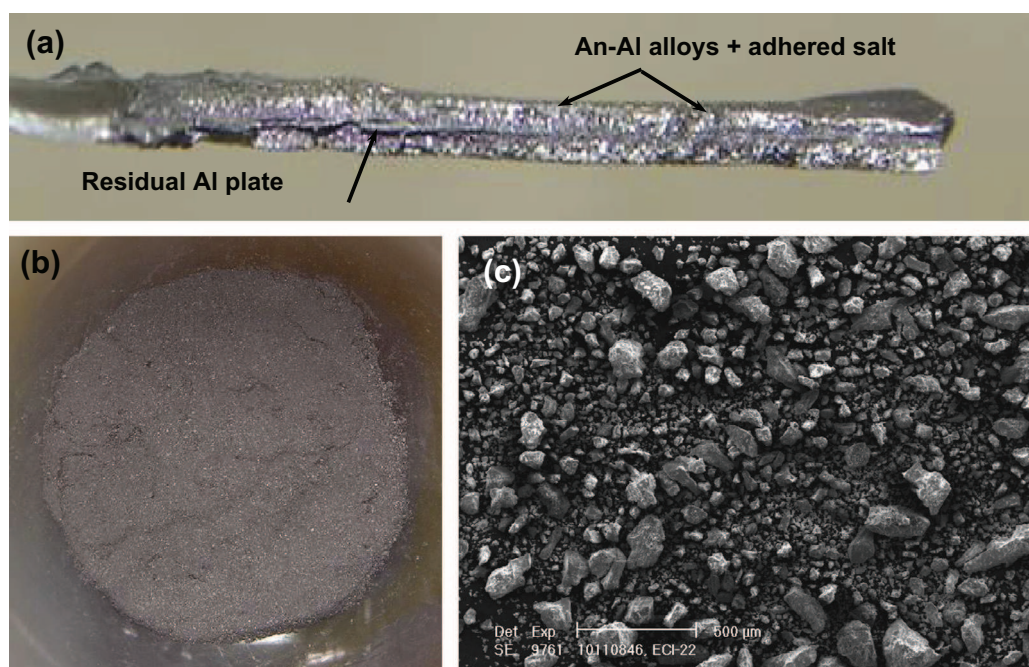

Fig. 3. (a) Cross section of the electrode from run 2 after the electrorefining (b) picture of the ground material prepared from run 2 (c) SEM micrograph of the ground material.

Table 1
Mass balance of the electrorefining runs for preparation of the An–Al alloys obtained by ICP-MS.

Run	Charge (C)	Mass of An (mg)		Ratio U/Pu	Current efficiency (%)	Loading (%)
		Expected	Analysed			
1	722	593.5	488.4	14.9	82.3	72.7
2	714	587.1	439.9	8.2	74.9	74.7
3	728	598.8	480.3	6.4	80.2	80.9

characterisation of the products made by XRD, selected samples were analysed by ICP-MS or ICP-OES and/or SEM-EDX according to the amount of the available material.

Although the precise grain distribution of the ground product was not evaluated, the SEM showed that the major part of the material was composed of 10–50 and 50–150 µm grains, in a ratio approximately 1:1, even though exceptionally larger particles were present. The maximum detected particle size was around 400 µm.

A picture of the ground material from run 2 and a SEM micrograph are shown in Fig. 3.

3. Chlorination experiments

Three chlorination runs were carried out individually for each material from runs 1 to 3 containing the electrochemically

prepared U–Pu–Al alloys and the adhered salt scraped from the electrode surfaces. The material, obtained from manually ground deposit to increase reaction surface, was used without sieving.

3.1. Experimental – chlorination

Due to their radiotoxicity and radioactivity, handling of actinide based samples during this study was done in a nitrogen glove-box equipped with a chlorine gas line, a vacuum system and a vertical furnace. A quartz reactor with sealed connections for gas inlets, outlets and a vacuum port was used and the processed materials were introduced in BN crucibles with inner diameter 30 mm. The experimental set-up is described in detail in the previous work [3]. Each run consisted of vacuum distillation, conversion to chlorides by two steps chlorination using gaseous Cl_2 and sublimation of the formed $AlCl_3$. The conditions for the three steps are summarised in Table 2 and they were kept the same for all processed materials.

3.2. Analyses

Samples of the processed materials were taken before and after each step and analysed by XRD according to the method described in [3] in order to evaluate distribution of the elements among the resulting phases. After a required treatment, e.g. homogenizing by grinding, the materials were transferred to a glove box with purified Ar atmosphere (<5 ppm moisture and oxygen), where the XRD samples were prepared. The samples of the material before chlorination, i.e., not containing $AlCl_3$, were embedded in an epoxy resin. All other samples were analysed in special low background and gas-tight holder ring dedicated to sensitive material from Bruker AXS (ref: A100-B139) to prevent reaction of $AlCl_3$ with the resin, which was observed during the previous work.

During this study, the material had to be sampled and partially processed under nitrogen atmosphere of the chlorination glove box. Nevertheless due to technical problem, the nitrogen atmosphere could contain some traces of oxygen and moisture. Based on previous experiments, it was proven that An–Al alloys are stable under the conditions of the samples processing and measurement, whereas samples containing chlorides are highly sensitive to traces of moisture and/or oxygen, forming oxychlorides, oxide and/or hydrates. Therefore, the oxy-compounds could be only formed from the chlorinated products and their presence can be used as a proof of successful chlorination.

3.3. Results and discussion

3.3.1. Salt distillation

About 700 mg of the initial material was introduced in the reactor, which was then evacuated to a pressure of $4\text{--}6 \times 10^{-2}$ mbar and heated to 800 °C. The distillation proceeded for 8 h, then the reactor was slowly cooled and pressurised at the room temperature. The set-up did not allow flushing the reactor by argon directly after the vacuum and it had to be filled with nitrogen atmosphere of the box. After sampling, the product was closed back to the reactor and kept under Ar flow. The appearance of the initial material changed from dark matt to more metallic shiny grey powder after the distillation, while the cold inner walls of the reactor were covered with a white condensate, which was recovered and analysed.

A mass balance of the distillation steps and an evaluation of the efficiency based on the mass loss of the material during distillation, XRD and ICP-MS results are summarised in Table 3. No direct analysis of Li, K and Cl was done by ICP-MS, whose results were used mainly to calculate the U/Pu ratio and the respective salt content was only approximately estimated by subtracting the measured concentrations of U, Pu and Al from 100 wt.%.

Fig. 4 reports the X-ray diffraction patterns of the starting material (top), the sample after distillation (middle) and of the condensate after distillation deposited on the internal wall of the reactor (bottom). The analysis indicated that the starting material was composed mainly of $AnAl_3$ (An: U, Pu) phases and the adhered LiCl–KCl salt. In addition, a relatively low content of $AnAl_4$ (An: U, Pu) was detected in some cases. After distillation (Fig. 4_middle), the pattern of the obtained material displays the absence of peaks corresponding to the salt LiCl or KCl, within the uncertainty limit of the method. The XRD analyses of the condensates (Fig. 4_bottom) yielded composition of pure LiCl–KCl and some other peaks which could be assigned to LiCl hydrate formed after absorption of moisture during the sample processing and measurement. ICP-MS analysis of the condensate from run 2 proved no volatilisation of actinides, however almost 2 wt.% of Al was detected in the condensate. It can be explained by presence of some pure Al metal (melting point 660 °C) in the initial material, originated probably from mechanical scraping of the deposit from the Al plate.

The complementary analyses of XRD and ICP-MS showed an excellent efficiency of the distillation step, as deposits containing initially about 20 wt.% of salt were successfully treated with An losses below the detection limit.

3.3.2. Chlorination and sublimation

About 300 mg of the product after distillation was used for chlorination. The powder was ground and introduced in the same BN crucible, the reactor was filled and flushed with Ar and heated to the desired working temperature 150 °C. After the temperature stabilised, Ar was substituted by pure Cl_2 at a flow rate of 35 ml/min and the reactor was flushed for 40 min. The gas was introduced directly above the surface of the material. The reactor was then isolated under chlorine and left for 20 h. After this reaction time, the reactor inlet and outlet were opened, Ar gas was introduced and in the same time, the reactor was slowly cooled. After reaching the room temperature, it was opened; the chlorination product was weighted, transferred to an agate mortar, manually ground and sampled. 300 mg of the product was as fast as possible put back into the reactor and the complete procedure was repeated for next 20 h using the same conditions.

The chlorination products from runs 1 and 2 consisted of homogeneously green powder, with no visually observable black metallic-like residues, as shown in Fig. 5. In addition, the products showed fully different properties than the initial material during mechanical treatment and sample preparation. Indeed it was easily ground with no resistance, which indicates absence of metallic grains, it adhered to the tools, it absorbed humidity from the glove box atmosphere and the powder samples were easily soluble in

Table 2
Description of the experimental procedure.

Step	Temperature (°C)	Time (h)	Conditions
Distillation	800	8	Reactor evacuated to $4\text{--}6 \times 10^{-2}$ mbar, heated, kept under vacuum
Chlorination	150	2×20	Reactor filled with pure Ar, heated, flushed with Cl_2 for 40 min at flow rate 35 ml/min, isolated
Sublimation	400	5	Reactor filled with pure Ar, heated, flushed constantly with Ar gas, flow rate 35 ml/min

Table 3
Mass balance of the salt distillation step Sample explanation: a – initial material, b – material after distillation, c – deposit condensed on the reactor walls during the distillation. Distribution of U and Pu phases in XRD results is evaluated using U/Pu ratio from the ICP-MS analyses.

| Run	Sample	Mass (mg)	Mass loss (%)	XRD (wt.%)							ICP-MS (2c: ICP-OES) (wt.%)				
				UAl_3	$PuAl_3$	UAl_4	$PuAl_4$	UAl_2	$PuAl_2$	LiCl–KCl	U	Pu	Al	Zr	LiCl–KCl
1	a	752.1	16.4	75.1	5.1	1.9	0.1	0.0	0.0	17.9	63.5	4.3	21.7	0.0	10.5
	b	628.6		80.4	5.6	0.0	0.0	13.1	0.9	0.0	69.7	4.8	22.4	0.0	3.2
2	a	682.3	22.7	75.5	9.2	0.1	0.0	0.0	0.0	15.2	54.2	6.6	18.7	0.6	19.9
	b	527.5		74.4	9.1	0.0	0.0	14.7	1.8	0.0	64.7	7.9	22.2	0.6	4.6
	c	n/a	–	0.0	0.0	0.0	0.0	0.0	0.0	100.0	0.0	0.0	1.8	0.0	97.5
3	a	720.3	12.1	65.7	10.2	0.0	0.0	0.0	0.0	24.1	57.7	9.0	23.8	0.1	9.4
	b	633.2		71.5	11.3	0.0	0.0	14.9	2.4	0.0	64.0	10.1	21.5	0.1	4.3
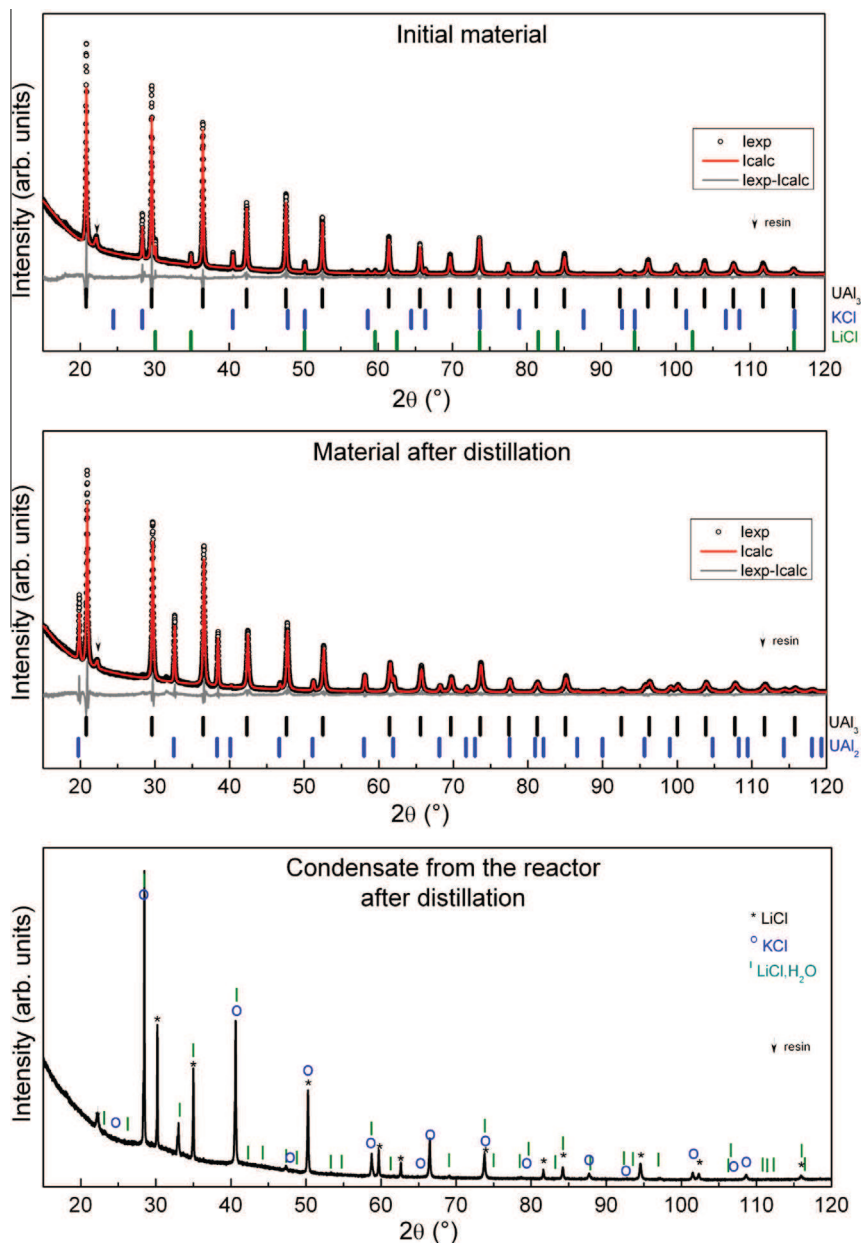
Fig. 4. XRD patterns of the initial material, the material after distillation and the condensate recovered from the cold parts of the reactor (first two patterns: circles – experimental points, lines – Rietveld data analyses, last pattern – experimental curve with phase analysis). The hydrate of LiCl observed in the condensate was formed during the analysis and XRD sample preparation.

$1\,M\,HNO_3$ with no insoluble residues. All these factors indicated a very high efficiency of the chlorination process.

During the chlorination of deposit from the electrode 3, technical problems with the under pressurised glove box occurred,

Fig. 5. Final product after the complete chlorination procedure (green sticky powder). (For interpretation of the references to colour in this figure legend, the reader is referred to the web version of this article.)

leading to oxidation of the material. Thus the data obtained by XRD could not be used to evaluate the process. The obtained product had black colour and it contained significant amount of UO_2 as determined by XRD analyses.

After sampling, all the remaining material was introduced back into the reactor in the same crucible and treated by sublimation. The reactor was closed, filled with Ar gas, flushed constantly using the same flow rate of 35 ml/min and heated to 400 °C. After 6 h, the reactor was slowly cooled down to the room temperature, opened to the nitrogen atmosphere of the glove box and the product was sampled. The appearance and properties of the products did not change after the sublimation step. A yellow-brownish condensate formed during the chlorination and sublimation steps on the cold reactor walls was scraped and analysed. The colour of the condensates indicated possible volatilisation of uranium, especially during run 1, for which a darker shade was observed.

A mass balance of the chlorination and sublimation steps and an evaluation of efficiencies is summarised in Table 4. The evaluation was based mainly on the Rietveld quantification of XRD results, which directly showed conversion rate of the alloys to chlorides. The representative XRD patterns of the material after first chlorination, sublimation and the condensate are compared in Fig. 6. As discussed above and in Section 3.2, the samples containing actinide and aluminium chlorides showed high moisture

affinity. All samples were processed, transported and measured under conditions not providing sufficient good quality and stability of the inert atmosphere. Therefore, some XRD measurements yielded too high noise/signal ratio and they could not be quantified by the Rietveld refinement method. The available results allow evaluation of the process, but not separate assessment of the individual steps. Therefore, the results of all steps including sublimation are presented together, showing the overall efficiencies.

The chlorination and sublimation products from run 1 were additionally analysed by ICP-MS. The analyses showed a slight decrease of Al content in the material after the sublimation step, but the detected Al concentrations were higher than expected, 17.1 and 6.4 wt.%, respectively. The final product from run 2 was therefore also additionally analysed and it confirmed high Al content in the chlorination and sublimation products, while the XRD analyses based only on the crystalline phases considered for the quantification showed only a minor content of phase with aluminium corresponding to UAl_3 as reported in Fig. 6 middle.

Due to the physical and chemical properties of the products indicating very high conversion ratio of the alloys to chlorides, it can be assumed that a major part of Al is present in the material as $AlCl_3$. This highly hygroscopic material was not detected by XRD, as it probably lost its crystal structure due to the reaction of the samples with moisture. This explanation is supported by a higher background of the XRD patterns observed for all the concerned samples, which can be explained by a presence of an amorphous phase. To determine its content in the sample, we used the program Topas version 4.1 considering all the peaks as crystalline phase and the broad peaks at high and low angle as the amorphous phase. The air scattering at low angle is limited through the use of sample holder equipped with a knife. The refinement evaluated 26 and 31 wt.% of amorphous content in the sublimation products. Assigning this to $AlCl_3$ only, the XRD results were in a good agreement with those found by ICP-MS. All these indicate higher chlorination efficiency, which was expected according to the last results on pure UAl_3 alloy using the same experimental conditions [3]. On the other hand, these results assume rather low efficiency of $AlCl_3$ sublimation step.

The condensates deposited on the cold parts of the quartz reactor after the chlorination and sublimation were recovered and analysed by XRD and ICP-MS. The XRD results yielded in both cases composition of pure $AlCl_3$. In this case, the sample was constituted mainly from $AlCl_3$ and the present humidity could not therefore transform the complete sample to an amorphous phase. However, the background observed for the previous samples was also detected and the intensity of signal was rather low, which indicates

Table 4

Mass balance of chlorination and sublimation steps Samples: a – initial material, b – material after 1st chlorination, c –material after 2nd chlorination d – material after sublimation, e – deposit condensed on the reactor walls during the chlorination and sublimation steps. Distribution of U and Pu phases in XRD results is evaluated using U/Pu ratio from the ICP-MS analyses.

Run	Sample	Mass (mg) before/after the exp. step	XRD (wt.%)								ICP-MS (wt.%)			
			UAl_3	$PuAl_3$	UAl_2	$PuAl_2$	UCl_4	UCl_3	$PuCl_3$	$AlCl_3$	U	Pu	Al	Zr
1	a	301.6	80.4	5.6	13.1	0.9	0.0	0.0	0.0	0.0	69.7	4.8	22.4	0.0
	b	391.8/302.0	6.5	0.5	0.0	0.0	86.0	1.5	5.5	0.0	n/a	n/a	n/a	n/a
	c	269.4/174.1	n/a	n/a	n/a	n/a	n/a	n/a	n/a	n/a	59.0	4.0	17.1	0.0
	d	150.8	2.4	0.2	0.0	0.0	59.6[a]	7.6	4.2	26.0	62.9	4.3	6.4	0.0
	e	n/a	0.0	0.0	0.0	0.0	0.0	0.0	0.0	100.0	2.0	0.0	14.8	0.0
2	a	300.4	74.4	9.1	14.7	1.8	0.0	0.0	0.0	0.0	64.7	7.9	22.2	0.6
	b	394.6/300.2	13.7	1.3	1.8	0.2	74.1	2.4	6.5	0.0	n/a	n/a	n/a	n/a
	c	329.8/201.0	n/a	n/a	n/a	n/a	n/a	n/a	n/a	n/a	n/a	n/a	n/a	n/a
	d	156.5	1.9	0.2	0.0	0.0	61.5[a]	0.0	5.4	31.0	54.5	5.5	9.4	0.2
	e	n/a	0.0	0.0	0.0	0.0	0.0	0.0	0.0	100.0	0.5	0.1	27.5	0.4

[a] Including $UOCl_2$ (1d) and UO_2 (2d) originating from reaction of UCl_4 with oxygen after the chlorination.
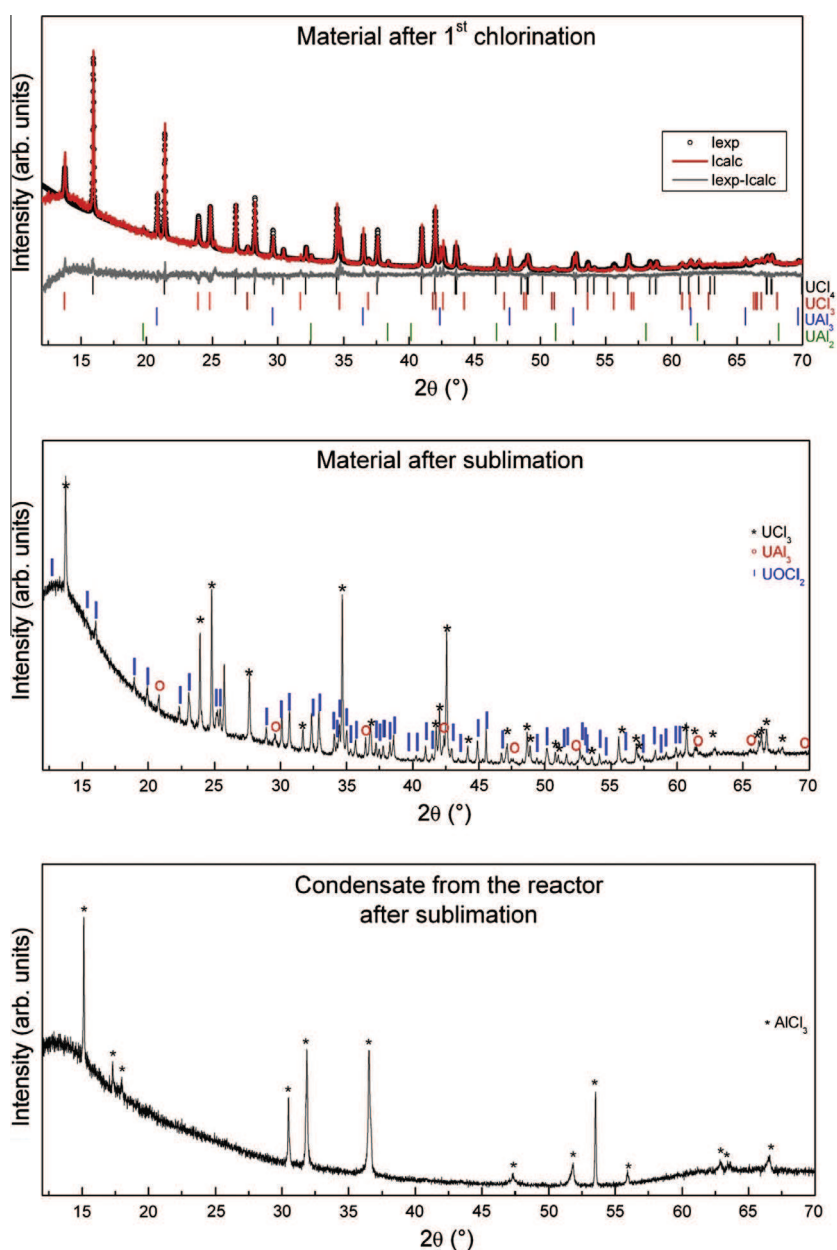
Fig. 6. XRD patterns of the material after 1st chlorination (top), sublimation (middle) and the condensate recovered from the cold parts of the reactor after sublimation (bottom). UOCl$_2$ detected in the sublimation product was probably formed during the sample preparation for XRD analysis.

formation of a thin layer of an amorphous phase on the sample surface. The ICP-MS measurements confirmed partial volatilisation of U as shown in Table 4. It indicates high sensitivity of the process to the working temperature, which should be further optimised. As shown in previous work [3], the volatilisation of U could very likely occur during the chlorination step, due to a slightly excessive working temperature.

4. Conclusions

The chlorination route described in the previous work [3] has been investigated using U–Pu–Al alloys prepared by electrochemical deposition of the actinides on solid Al plates in molten LiCl–KCl. The initial material contained the salt adhered on the surface and in the pores of the formed deposits. All steps of the process

have been experimentally tested and evaluated using a combination of different analytical techniques.

In addition to a verification of some parameters of the electrorefining process for recovery of actinides from U–Pu–Zr alloy based fuel, the study has yielded the following main conclusions on the chlorination route:

- The vacuum salt distillation process is very efficient at the given conditions, i.e., temperature 800 °C and vacuum 5×10^{-2} mbar. The experiments have shown that the salt can be completely removed without actinide loss.
- The chlorination step also seems to be very efficient, but the conversion ratio could not have been exactly evaluated. The quantifications of the XRD patterns have yielded conversion efficiencies 97–98%, assuming that amorphous phases in the patterns are associated only with pure AlCl$_3$. This assumption is supported by ICP-MS results, which have yielded significantly

higher Al content in the chlorination products than detected by the analysis of the crystalline phases of the XRD patterns. The appearance, physical and chemical properties of the products indicated low or no content of the initial metallic alloy material. Therefore, it have been concluded that the products contain amorphous $AlCl_3$, however the exact distribution of Al between An–Al alloys and $AlCl_3$ cannot be in principle determined from the available data.

– The sublimation efficiency seems to be relatively low, but cannot be exactly evaluated, due to the facts discussed above.
– It seems that uranium has been partly volatilised, as up to 2 wt.% of U has been detected in the condensate deposited on the reactor cold walls during the chlorination and sublimation steps. Since no U has been volatilised during the previous experiments using UAl_3 initial material at the same experimental conditions, it indicates very high sensitivity of the process to the working temperature. No influence of Pu on U volatilisation is expected and the probable explanation is variations of temperature during the chlorination experiment, especially in run 1. In the condensates from other runs, only 0.5 and 0.3 wt.% U was detected.

The results have indicated that the chlorination route is a very promising method, however the sublimation step has to be further optimised and a precise temperature control is needed. Both these factors can be advantageously influenced by using HCl gas instead Cl_2. Due to preliminarily thermodynamic calculations, the chlorination using HCl gas can be carried out at significantly higher temperatures without volatilisation of actinides, up to 400 °C. It would very likely enhance sublimation of $AlCl_3$ directly during the chlorination step and the process would be more robust to temperature changes.

Acknowledgements

References

[1] J. Serp, M. Allibert, A. Le Terrier, R. Malmbeck, M. Ougier, J-P. Glatz, J. Elect. Soc. 152 (2005) 167–172.
[2] P. Souček, R. Malmbeck, E. Mendes, C. Nourry, J.-P. Glatz, Recovery of Actinides from Spent Nuclear Fuel by Pyrochemical Reprocessing, in: Proceedings of Global 2009, Paris, September 6–11, 2009, pp. 1156–1165.
[3] L. Cassayre, P. Soucek, E. Mendes, R. Malmbeck, C. Nourry, R. Eloirdi, J.P. Glatz, J. Nucl. Mater. 414 (1) (2011) 12–18.
[4] P. Souček, R. Malmbeck, C. Nourry, J.P. Glatz, Energy Procedia 7 (2011) 396–404.
[5] P. Souček, L. Cassayre, R. Malmbeck, E. Mendes, R. Jardin, J.-P. Glatz, Radiochim. Acta 96 (2008) 315–322.
[6] L. Cassayre, C. Caravaca, R. Jardin, R. Malmbeck, P. Masset, E. Mendes, J. Serp, P. Souček, J.-P. Glatz, J. Nucl. Mater. 378 (2008) 79–85.
[7] E. Mendes, R. Malmbeck, C. Nourry, P. Souček, J.P. Glatz, J. Nucl. Mater. 420 (2012) 424–429.
[8] M. Iizuka, K. Kinoshita, T. Koyama, J. Phys. Chem. Solids 66 (2005) 427–432.